

ORIGINAL RESEARCH ARTICLE

Construction of prognostic risk models and identification and verification of biomarkers related to lactic acid metabolism and carbohydrate metabolism in lung adenocarcinoma

Zhiping Zhao^{ID}, Jiande Cheng^{ID}, and Yanyan Hao*^{ID}

Department of Respiratory and Critical Care Medicine, Third Hospital of Shanxi Medical University, Shanxi Bethune Hospital, Shanxi Academy of Medical Sciences; Tongji Shanxi Hospital, Tongji Medical College, Huazhong University of Science and Technology, Taiyuan, Shanxi, China

Abstract

Lung adenocarcinoma (LUAD) has a high incidence and poor prognosis. Carbohydrate and lactic acid metabolism drive tumor growth, highlighting the need to identify prognostic genes in these pathways for LUAD diagnosis and treatment. We conducted differentially expressed analysis in the Cancer Genome Atlas (TCGA)-LUAD, applied Spearman analysis to correlate carbohydrate and lactic acid metabolism genes and identified key model genes using weighted gene co-expression network analysis. Overlapping differential expression genes (DEGs), correlated genes, and key model genes yielded candidates. Hub genes were screened by molecular complex detection, prognostic genes by univariate Cox, and least absolute shrinkage and selection operator, constructing a risk model. TCGA-LUAD samples were stratified by median risk score. Finally, the prognostic genes' impact on LUAD's immune microenvironment was analyzed, and their expression in clinical samples was validated through real-time quantitative polymerase chain reaction. From 7,252 DEGs, 189 correlated genes, and 3,900 key model genes, 20 candidates emerged. Nine hub genes led to five prognostic genes: *ADH1A*, Alcohol dehydrogenase 1B (*ADH1B*), *ALDOA*, *ENO1*, and *ACSS3*. In addition, nine immune cells differed significantly between risk groups, with CD4 T, monocytes, and mast cells positively correlating with *ADH1B*. *ADH1A*, *ADH1B*, and *ACSS3* were downregulated, contrasting *ALDOA* and *ENO1*. Consistent results were obtained by protein mapping. Eventually, *ADH1A*, *ADH1B*, *ALDOA*, and *ENO1* expression trends in clinical samples were similarly consistent with the dataset. In summary, five prognostic genes related to carbohydrate and lactic acid metabolism (*ADH1A*, *ADH1B*, *ALDOA*, *ENO1*, and *ACSS3*) associated with LUAD have been identified. This model serves as an effective predictive tool and offers a new perspective for studying tumor metabolism.

Keywords: Lung adenocarcinoma; Carbohydrate metabolism; Lactic acid metabolism; Prognostic genes

***Corresponding author:**

Yanyan Hao
(yanyan.hhao@gmail.com)

Citation: Zhao Z, Cheng J, Hao Y. Construction of prognostic risk models and identification and verification of biomarkers related to lactic acid metabolism and carbohydrate metabolism in lung adenocarcinoma. *Cancer Plus*. 2025;7(1):43-63. doi: 10.36922/cp.5992

Received: November 15, 2024

Revised: February 21, 2025

Accepted: March 5, 2025

Published online: April 7, 2025

Copyright: © 2025 Author(s). This is an Open-Access article distributed under the terms of the Creative Commons Attribution License, permitting distribution, and reproduction in any medium, provided the original work is properly cited.

Publisher's Note: AccScience Publishing remains neutral with regard to jurisdictional claims in published maps and institutional affiliations.

1. Introduction

It is a widely known fact that lung adenocarcinoma (LUAD) tends to have a poor prognosis.^{1,2} Notably, different histological subtypes of LUAD exhibit significant variability in the extent of immune cells.³ In practical medical scenarios, considering the individual variability of patients, it is difficult to accurately assess the prognosis by solely relying on histopathology. Therefore, a multivariate biomarker strategy becomes necessary to predict the survival duration of lung cancer patients more accurately. The predictive power of a single gene is stretched in lung cancer prognosis. On the contrary, the integration of multiple predictors improves the accuracy of prediction and enhances the sensitivity and specificity of prognostic judgment in lung cancer.⁴ Currently, treatment is mainly a combination of targeted therapy and immunotherapy. Nevertheless, the late diagnosis and the fact that the tumor exhibits inherent or acquired drug resistance results in a still poor prognosis for LUAD, with a survival rate of only 15% at 5 years.⁵ The late diagnosis of tumors and the development of primary and secondary drug resistance contribute to the poor prognosis of lung adenocarcinoma. It is of vital importance to identify biomarkers that can enable early diagnosis and accurate prediction of the prognosis of lung cancer.

To adapt to the environment, tumor cells undergo alterations in their carbohydrate and lipid metabolism to acquire essential nutrients for energy production and growth. These metabolic adaptations enhance the survival, proliferation, and metastasis of tumor cells.⁶ Metabolic reprogramming is the key to tumor recurrence, and its main function is to provide sufficient energy for rapidly dividing tumor cells.⁷ In cancer evolution and recurrence, carbohydrate metabolism has a key impact on tumor growth, angiogenesis, distal spread, invasive properties, and treatment resistance.^{8,9} Studies conducted in various experimental models have reported that alterations in carbohydrate metabolism precede the onset of numerous tumorigenic processes and exhibit a close association with the transformation of tumor cells.¹⁰ Lactate is also an important factor in tumor metabolism, and certain cancer cells opt for anaerobic glycolysis to metabolize glucose even under oxygen-sufficient conditions.^{11,12} Anaerobic glycolysis of cancer cells generates lactate, which creates an acidic environment that promotes tumor growth and metastasis.¹³ Lactic acid not only provides energy for tumor tissues but also regulates the immune response in the tumor microenvironment.¹⁴ Studies indicate that lactate strengthens regulatory T cells (Tregs) in the tumor microenvironment.¹⁵ The expression of lactate and lactate dehydrogenase promotes metabolic adjustments in cancer cells, which in turn aids in tumor formation. There is an intricate network of associations involving glucose

metabolism, lactate production, and regulation of immune responses.¹⁶ Understanding the biological mechanisms of aerobic glycolysis and its regulatory pathways provides new directions for the development of glycolysis-based cancer therapeutic strategies. Combining glycolysis inhibitors with DNA-damaging drugs or chemotherapeutic agents can effectively inhibit the damage repair function of cancer cells and enhance the cytotoxic effect of the drugs, forming a powerful anticancer tool.¹⁷ Exploring the role of carbohydrate metabolism and lactic acid metabolism in tumors could be beneficial for the development of new drugs for LUAD.

Due to the significant roles of carbohydrate metabolism and lactic acid metabolism in tumors, we plan to utilize bioinformatics methods to explore the importance of metabolism-related genes in LUAD. In addition, in clinical practice, subtypes of lung cancer and individual tumor markers are unable to accurately predict the prognosis of LUAD. Therefore, this study intends to explore prognostic genetic profiles using risk models to more accurately predict the prognosis of LUAD.

2. Methods

2.1. Data collection

Data on LUAD patients were extracted from the Cancer Genome Atlas Program (TCGA) database, which included the RNA-sequencing data, copy number variation (CNV), and clinical information of 510 tumor samples and 58 normal tissue samples. GSE31210, including 226 LUAD and 20 normal tissue samples, was obtained from the Gene Expression Omnibus (GEO) database. A total of 353 carbohydrate metabolism-related genes (CRGs)¹⁸ were collected from previous research, and 15 lactic acid metabolism-related genes (LRGs) were gained from the Molecular Signatures Database (MSigDB) (<https://www.gsea-msigdb.org/gsea/msigdb>).

2.2. Weighted gene co-expression network analysis (WGCNA)

The WGCNA package (v1.7.1)¹⁹ was used in this study to obtain gene modules associated with LUAD. The clustering of TCGA-LUAD samples was carried out to detect whether there were outlier samples. Then, the optimal soft threshold (β) was performed. The co-expression matrix was established, identifying gene modules and labeling them with different colors. The modules most relevant to the existence of LUAD were considered critical modules, and their related genes were the key module genes.

2.3. Differential expression and correlation analysis

The differential expression genes (DEGs) were obtained through differential expression analysis (DESeq2, v1.34.0)²⁰

with $|\log_2FC| > 1$ and adjusted $p < 0.05$ between LUAD and normal samples in TCGA-LUAD. In addition, Spearman correlation analysis of CRGs and LRGs was performed by Hmisc (v5.1.0),²¹ and the correlated genes were screened with $p < 0.05$ and $|r| > 0.3$. Subsequently, DEGs, key module genes, and correlated genes overlapped as candidate genes. Then, the functions involved in DEGs and candidate genes were further explored through enrichment analysis (clusterProfiler, v4.6.0),²² respectively.

2.4. Identification of prognostic gene

To observe the relationship between candidate genes, a protein-protein interaction (PPI) network was established. After that, the molecular complex detection (MCODE) algorithm was utilized to screen hub genes in candidate genes for subsequent analysis (degree cutoff = 2; maximum depth = 100; k core = 2; node score cutoff = 0.2). Furthermore, univariate Cox regression analysis and least absolute shrinkage and selection operator (LASSO, glmnet [v4.1.4])²³ were further performed on hub genes to screen out prognostic genes, and a prognostic risk model was constructed.

$$\text{Risk score} = \sum_1^n \text{coef}(\text{genei}) * \text{expression}(\text{genei}) \quad (\text{I})$$

Patients in the TCGA-LUAD dataset were categorized into high-risk and low-risk groups based on median risk scores.

2.5. Risk model

Using the Kaplan-Meier (KM) curve can effectively compare the survival of the high- and low-risk groups and clarify the group differences in survival using the “survival” package (v3.5 – 5).²⁴ In addition, survival receiver operating characteristic (ROC) (v1.0.3.1)²⁵ was used to plot the ROC curve of patients at 1, 3, and 5 years to evaluate the effectiveness of the risk model. Finally, the risk model was verified in GSE31210 for the accuracy of the results.

2.6. Independent prognostic analysis and construction of alignment chart

Risk scores and clinical features of LUAD patients were integrated to screen for independent prognostic factors. First, univariate Cox independent prognostic analysis was executed using the “survival” package; proportional hazards (PH) tests ($p > 0.05$) were then performed on factors with $p < 0.05$. Finally, factors that passed multivariate Cox independent prognostic analysis were identified as independent prognostic factors ($p < 0.05$), and an alignment chart was constructed; the 1-, 3-, and 5-year survival rates were predicted by the overall score. Furthermore, the ROC curve, calibration curve, and decision curve analysis

(DCA) were applied to evaluate the validity and reliability of the alignment chart.

2.7. Gene set variation analysis (GSVA) and gene set enrichment analysis (GSEA)

To explore the KEGG pathway differences between the high- and low-risk groups, GSVA was performed using the GSVA package (v1.46.0)²⁶ with the TCGA-LUAD dataset. The enrichment scores for each signaling pathway were calculated with reference to the “C2: KEGG gene sets” gene set in the MSigDB database. Subsequently, the limma package (v3.54.1)²⁷ was used to compare the pathway differences between the high- and low-risk groups, and the top 20 enriched pathways were displayed with the filter condition of $\text{adj.p.val (false discovery rate [FDR])} < 0.05$. In addition, GSEA²⁸ was performed to analyze the functions and pathways involved in prognostic genes. First, the fold changes of all genes in the high- and low-risk groups were calculated by limma (v3.54.1)²⁷ and then sorted. For GSEA, “c2.cp.kegg.v2023.1.Hs.symbols.gmt” was used as the reference gene. Finally, pathways with $p < 0.05$ were considered statistically significant.

2.8. Immune infiltration analysis and CNV

As many studies have demonstrated that lactic acid accumulation in tumors affects immune cell function, we performed immune cell infiltration analysis in the high- and low-risk groups. Regarding differential immune cells, the distribution ratio of 22 kinds of immune cells in TCGA-LUAD samples was observed. The Wilcoxon test ($p < 0.05$) was applied to screen immune cells with significant differences between the two risk groups, and the correlation between them was analyzed. Finally, Spearman analysis ($|r| > 0.3$; $p < 0.05$) was utilized to explore the association between differential immune cells and prognostic genes. In addition, the CNV of the two risk groups was analyzed through Genepattern (<https://cloud.genepattern.org/>).

2.9. Regulation mechanism

To analyze the potential regulatory mechanisms of prognostic genes in LUAD, the transcription factors (TFs) corresponding to prognostic genes were predicted in regulon, while the corresponding miRNAs were predicted in the miRNet database. The TF-mRNA-miRNA regulatory network was then constructed. Subsequently, correlations between prognostic genes and TFs were explored using Spearman correlation analysis in the TCGA-LUAD dataset.

2.10. Expression analysis

Prognostic gene expression levels were confirmed through multi-level verification. The expression patterns

within TCGA-LUAD were showcased in box plots and cross-validated using protein mapping. In addition, the expression of prognostic genes was verified by reverse transcription-quantitative polymerase chain reaction (RT-qPCR). A total of 10 pairs of normal and LUAD samples were obtained from the clinic in the Shanxi Bethune Hospital (China). Informed consent was obtained from all participants, and the study was approved by the Shanxi Bethune Hospital Medical Ethics Committee (YXLL-2024-082).

The extraction of total RNA from the 20 specimens was carried out using TRIzol reagent (Invitrogen, China), strictly adhering to the manufacturer's guidelines. Subsequent quantification of RNA concentrations was facilitated using the NanoPhotometer N50 (Implen, Germany). Complementary DNA (cDNA) synthesis was achieved through reverse transcription, employing the SureScript First-strand cDNA synthesis kit (Servicebio, China). qPCR was executed on a CFX Connect Thermal Cycler (Bio-Rad, United States of America [USA]). For the relative quantification of mRNA levels, the $2^{-\Delta\Delta CT}$ method was utilized. The primer sequences employed in the study are listed in Table S1.

2.11. Statistical analysis

If not otherwise stated, the p -value was calculated using the Wilcoxon test: *** $p < 0.001$, ** $p < 0.01$, and * $p < 0.05$.

3. Results

3.1. Identification of 3,900 key model genes, 7,252 differentially expressed genes, and 189 correlated genes

There were no obvious outliers in the TCGA-LUAD sample (Figure A1). The soft threshold (β) was selected as 4 to achieve scale-free topology (scale-free $R^2 > 0.85$) (Figure 1A), and 15 co-expression modules were identified (Figure 1B). Among these, the blue model ($|r| = 0.77$; $p = 5 \times 10^{-114}$) was most related to LUAD and regarded as a key model (Figure 1C); it was involved in 3,900 genes.

A total of 7,252 DEGs were identified between LUAD and normal samples, comprising 4,842 upregulated and 2,410 downregulated genes (Figure 1D and E). GO analysis suggested that they were mainly enriched in development and morphogenesis, followed by transport and cell adhesion (Figure 1F). KEGG analysis indicated that these genes were involved in ABC transporters, cytokine-cytokine protein receptor interactions, and cytochrome P450-mediated metabolism (Figure 1G). In addition, 189 correlated genes were obtained from 353 CRGs and 15 LRGs by correlation analysis (Table S2).

3.2. Identification and function analysis of 20 candidate genes

The 20 candidate genes were acquired through the intersection of correlated genes, DEGs, and key model genes (Figure 2A). Meanwhile, these genes were mainly enriched in metabolic processes, including carbohydrate and polysaccharide synthesis (Figure 2B), as well as glycolysis/gluconeogenesis, fructose metabolism, amino acid biosynthesis, pyruvate metabolism, and mannose metabolism (Figure 2C). Notably, there was a certain interaction between them; for example, *HMGCS1* was associated with most genes, such as *ADH1A*, *ACSS3*, *ACACB*, and *ADH1B* (Figure 2D). *ENO1*, a key enzyme in glycolysis, interacts with *ADH1A*, *ADH1B*, *ACSS3*, *ALDOA*, and other proteins, suggesting a synergistic role in cell metabolism, signal transduction, and other physiological processes (Figure 2D).

3.3. Acquisition of five prognostic genes and construction of risk models

Nine hub genes were selected by the MCODE algorithm for subsequent analysis (Figure 3A). The proteins encoded by key genes involved in glucose metabolism (*ADH1A*, *ALDOA*, *ACSS3*, *IDH2*, *ACACB*, *ADH1B*, and *ENO1*) exhibit interaction relationships, suggesting potential synergistic or regulatory connections in the cell physiological process. Five prognostic genes (*ADH1A*, *ADH1B*, *ALDOA*, *ENO1*, and *ACSS3*) were obtained by univariate Cox (Figure 3B) and LASSO (lambda.min = 0.0023) (Figure 3C) and used to construct a risk model. The protein expression of these five key genes was predicted using the density map of protein expression data distribution. Among them, *ACSS3* exhibited the highest expression level, while *ADH1A* had the lowest (Figure 3D).

3.4. Construction of an effective model

The distribution of patients in the two risk groups in TCGA-LUAD is displayed in Figure 4A. The KM curve indicated that the survival rate of patients in the high-risk group was significantly lower than that of patients in the low-risk group (Figure 4B). In addition, the area under the curve (AUC) value was > 0.6 (1-year: 0.609; 3-year: 0.634; 5-year: 0.630), indicating that the effect of the model was prominent (Figure 4C). Moreover, the heat map demonstrated that *ALDOA* and *ENO1* were greatly expressed in the high-risk group, while *ACSS3*, *ADH1A*, and *ADH1B* were greatly expressed in the low-risk group (Figure 4D). The validity of the risk model was also demonstrated in the validation set (GSE31210) (Figure 4E-H).

3.5. Independent prognostic factors are risk score and stage

Risk score and stage were found to be independent prognostic factors using three methods (univariate Cox

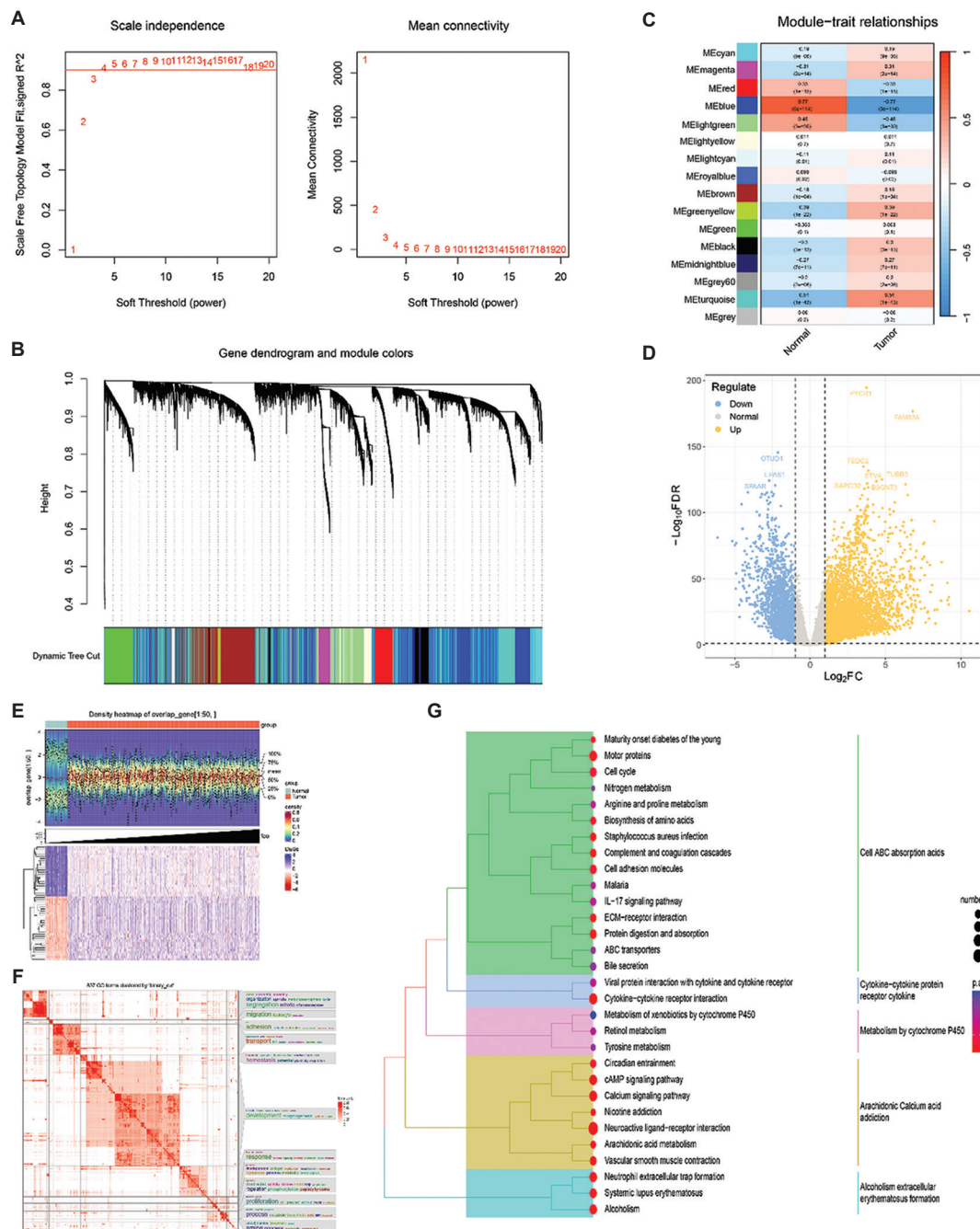


Figure 1. Identification of 3,900 key model genes, 7,252 DEGs, and 189 correlated genes. (A) Selection of the soft threshold β . Both horizontal axes represent the weight parameter power value; the vertical axis of the left panel represents the scale-free fit index (i.e., signed R^2); and the vertical axis of the right panel represents the mean value of the neighbor-joining function of all genes in the corresponding gene module. (B) Module clustering diagram. The top half of the diagram represents a hierarchical clustering dendrogram of genes, while the bottom half represents a gene module. The top and bottom segments correspond to each other, where genes clustered to the same branch are classified into the same module, and different colors represent different modules. (C) Heatmap of the relationship between gene modules and traits. A darker color indicates a higher correlation; red denotes a positive correlation, while blue denotes a negative correlation. Numbers in the cells indicate correlation and significance, with correlation in the top row and p -value (significance) in the bottom row. (D) Volcano map of differentially expressed genes. Each point in the plot represents a gene; yellow represents upregulated differentially expressed genes; blue represents downregulated differentially expressed genes; and gray represents non-significantly differentially expressed genes. (E) Heatmap of differentially expressed genes. Purple color denotes a high expression, while red color denotes a low expression. (F) GO enrichment analysis of differentially expressed genes. (G) KEGG enrichment analysis of differentially expressed genes. Abbreviations: DEGs: Differentially expressed genes; GO: Gene ontology.

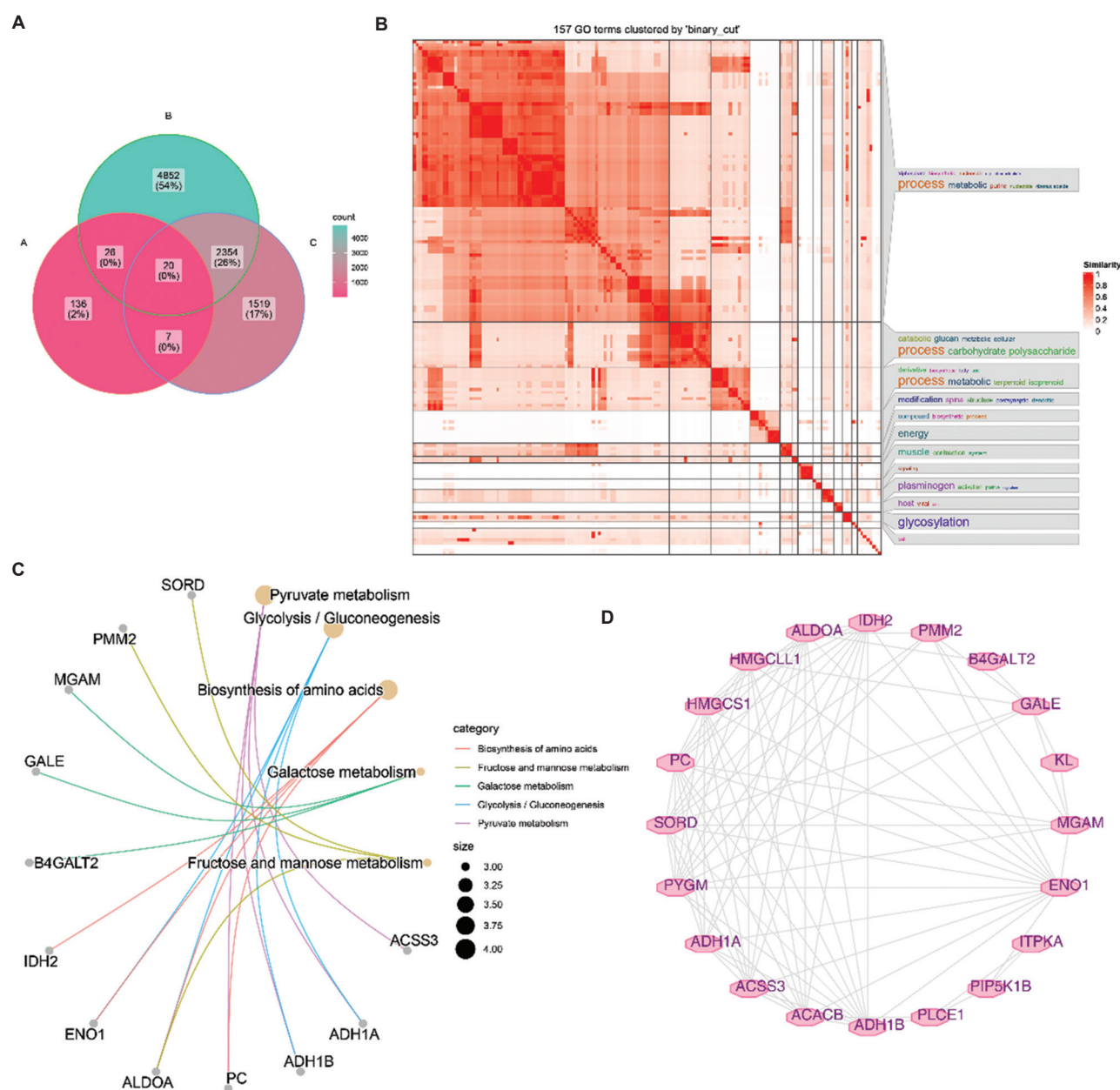


Figure 2. Identification and function analysis of 20 candidate genes. (A) Venn diagram of the intersection of correlated genes, DEGs, and key model genes. (B) GO enrichment analysis of candidate genes. (C) KEGG enrichment analysis of candidate genes. (D) PPI network of candidate genes. Abbreviations: DEG: Differentially expressed genes; GO: Gene ontology; KEGG: Kyoto encyclopedia of genes and genomes; PPI: Protein-protein interaction.

regression analysis, PH test. multivariate Cox regression analysis) (Figure 5A-C). An alignment chart was plotted to forecast the 1-, 3-, and 5-year survival rates of patients using risk score and stage (Figure 5D); the higher the total score, the lower the survival rate. Meanwhile, AUC values were >0.6 (1-year: 0.750; 3-year: 0.729; 5-year: 0.683) (Figure 5E); DCA analysis revealed that the alignment chart had the best net benefit (Figure 5F). Similarly, the calibration curve coincided with the ideal

curve (Figure 5G), indicating that the alignment chart had excellent predictive ability.

3.6. Functional enrichment of prognostic gene

To explore pathway differences between the two risk groups, GSEA indicated that eight pathways were greatly expressed in the low-risk group (including ABC transporters, ether lipid metabolism, and complement and coagulation cascades), while 12 pathways were highly expressed in

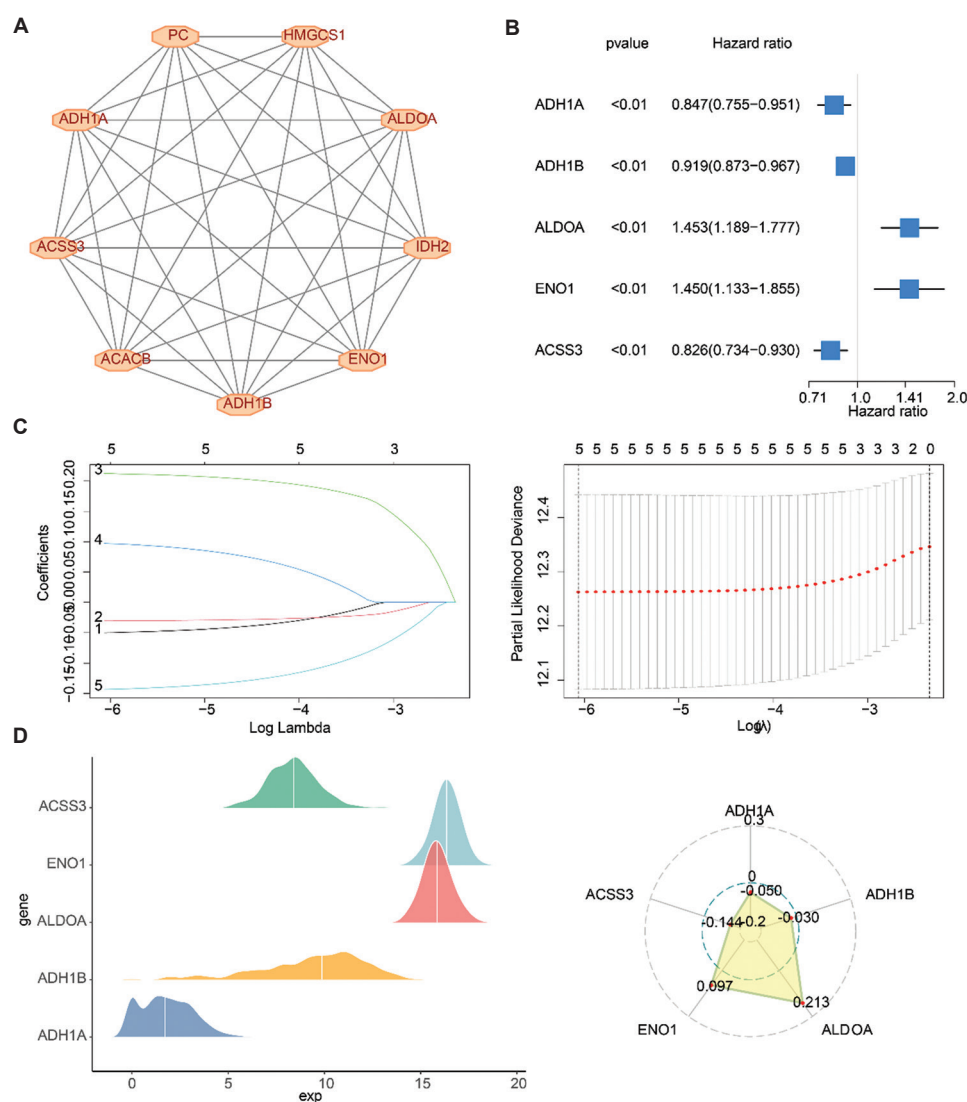


Figure 3. Acquisition of five prognostic genes and construction of risk models. (A) The PPI network of hub genes. (B) Univariate Cox forest plot. The left side represents genes and the corresponding p and HR values; the blue squares on the right side indicate HR values <1 or >1 , and the lines on either side of the squares are the 95% confidence intervals for the HR values. (C) LASSO results map. Each curve in the left plot represents the trajectory of each coefficient of the independent variable, the vertical coordinate is the coefficient value, and the horizontal coordinate is the number of non-zero coefficients in the model at this point. The horizontal coordinate of the right plot is $\log(\text{Lambda})$, and the vertical coordinate represents the cross-validation error. (D) Prognostic gene expression levels and characterization coefficients. Different colored modules represent the expression levels of different prognostic genes.

Abbreviations: PPI: Protein-protein interaction; LASSO: Least absolute shrinkage and selection operator.

the high-risk group (such as glyoxylate and dicarboxylate metabolism, and the pentose phosphate pathway [PPP]) (Figure 6A). In addition, the prognostic genes involved in the related pathways were analyzed. *ADH1A* (Figure 6B), *ADH1B* (Figure 6C), and *ACSS3* (Figure 6D) were significantly enriched in the spliceosome, cell cycle, and neuroactive ligand-receptor interaction pathways, while *ALDOA* (Figure 6E) and *ENO1* (Figure 6F) were significantly enriched in oxidative phosphorylation and ribosome pathways.

3.7. Differential immune infiltration and CNV

Changes in lactic acid metabolism can alter the activity of immune cells.²⁹ To further analyze the effect of prognostic genes in the LUAD immune microenvironment, the distribution ratio of 22 types of immune cells was analyzed (Figure 7A). All nine differential immune cells acted as key immune infiltrating cells (Figure 7B). Among them, resting mast cells, naive B cells, monocytes, and resting memory CD4 T cells were upregulated in

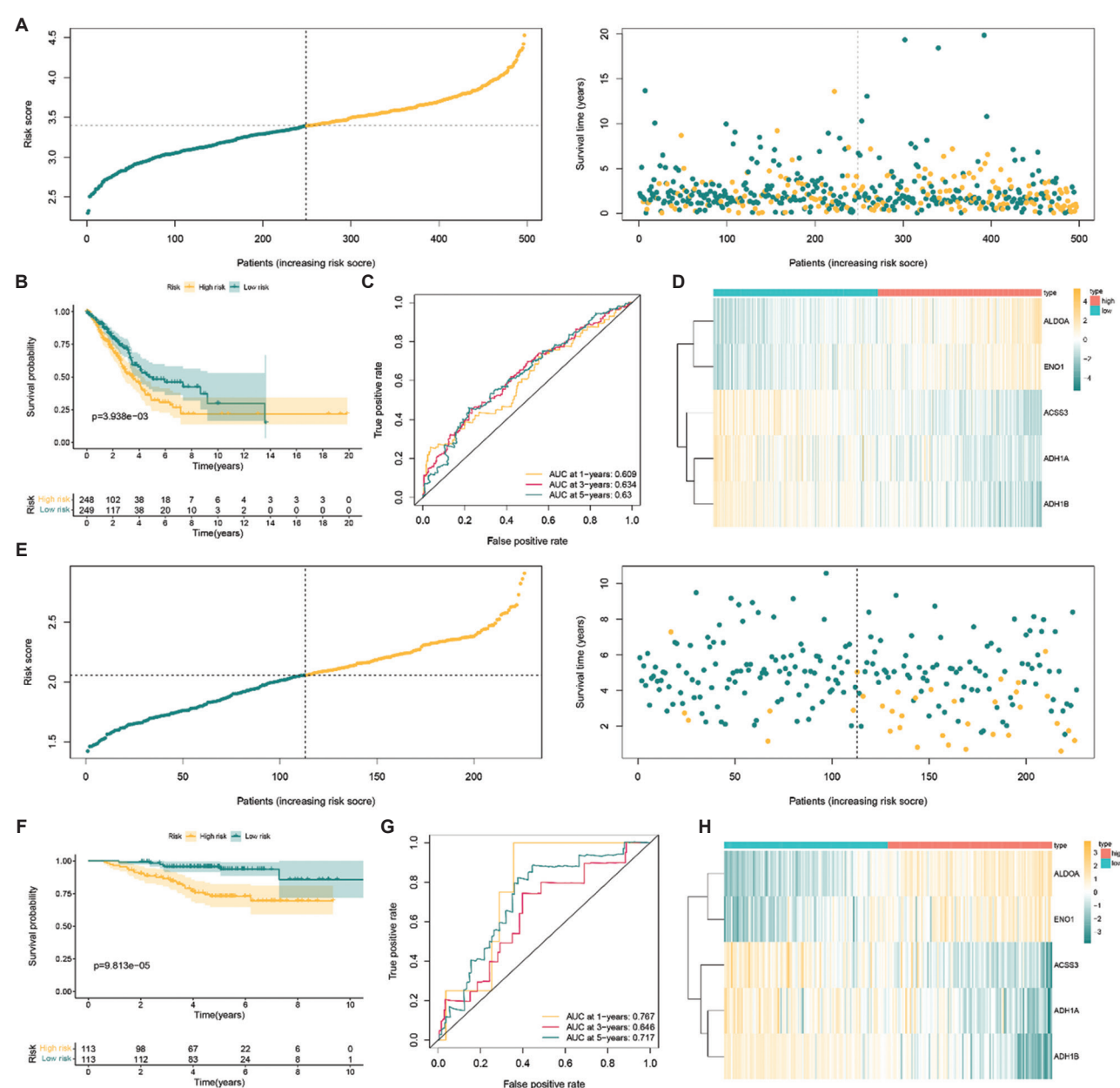


Figure 4. Construction of an effective model. (A) Survival differences between high- and low-risk groups in the training set. Green denotes a low risk; yellow denotes a high risk. (B) KM curve for high- and low-risk groups in the training set. It can be seen that the survival probability of the high-risk group decreases faster, while the survival probability of the low-risk group decreases relatively slowly. (C) ROC curves at 1, 3, and 5 years for high- and low-risk groups in the training set. (D) Heatmap of expression of prognostic genes in high- and low-risk groups in the training set. (E) Survival differences between high- and low-risk groups in the validation set. (F) KM curve for high- and low-risk groups in the validation set. (G) ROC curves at 1, 3, and 5 years for high- and low-risk groups in the validation set. (H) Heatmap of expression of prognostic genes in high- and low-risk groups in the validation set. Abbreviations: KM: Kaplan-Meier; ROC: Receiver operating characteristic.

the low-risk group, whereas helper follicular T cells, M0 macrophages, Tregs, and M1 macrophages were upregulated in the high-risk group. Meanwhile, in the high-risk group, resting mast cells displayed a remarkably negative correlation with activated mast cells (correlation coefficient [cor] = -0.49 ; $p < 0.001$),

and monocytes had a signally positive correlation with resting mast cells ($\text{cor} = 0.32$; $p < 0.001$). In the low-risk group, M0 macrophages displayed a negative correlation with monocytes ($\text{cor} = -0.35$; $p < 0.001$), while there was a markedly positive association between monocytes and resting mast cells ($\text{cor} = 0.41$; $p < 0.001$) (Figure 7C).

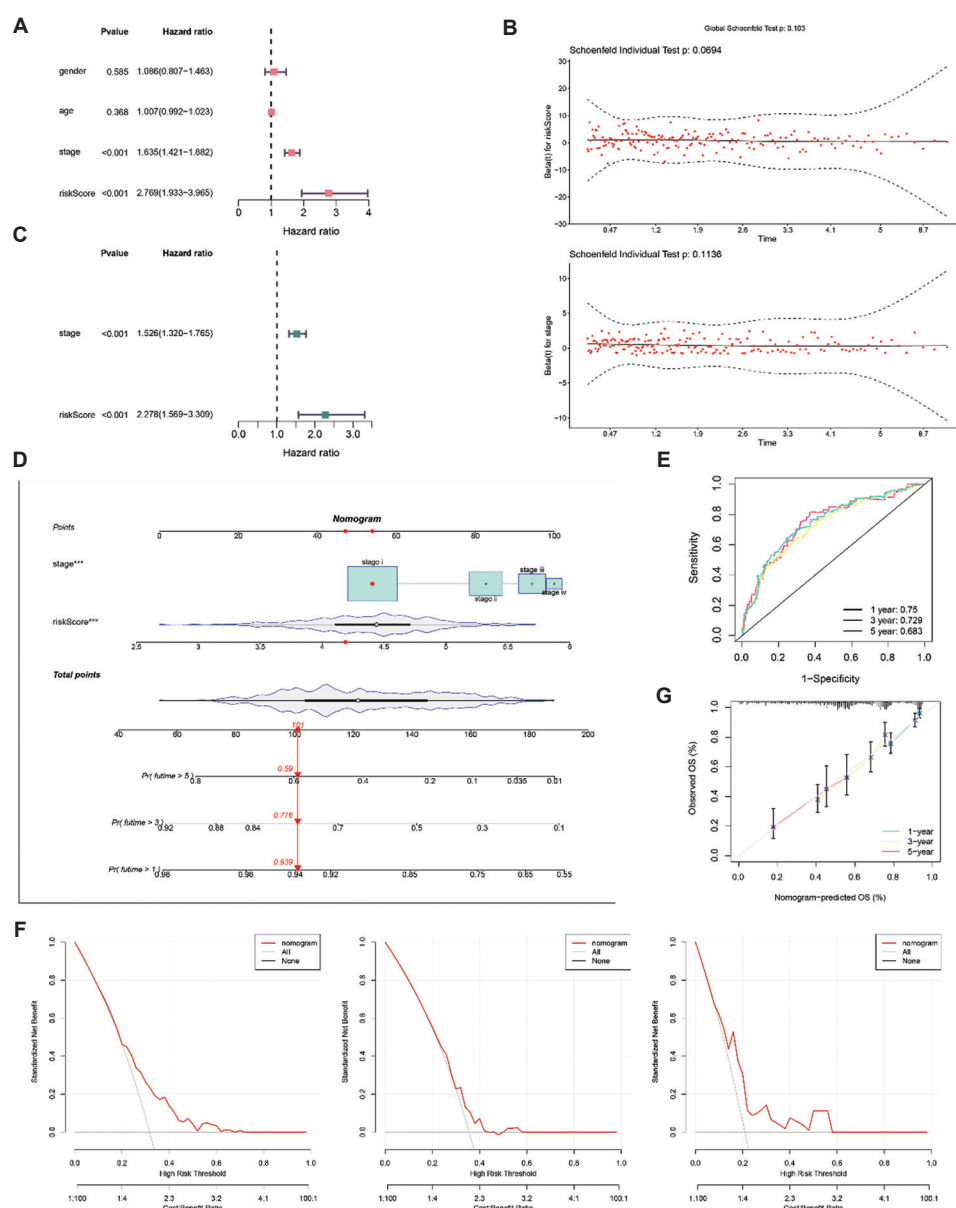


Figure 5. Independent prognostic factors are risk score and stage. (A) Results of univariate Cox regression analysis. Gender and age had no significant influence on survival, while disease stage and risk score had significant influence on survival, which were considered risk factors. (B) Results of the PH test. (C) Results of multivariate Cox regression analysis. In the multifactor model, disease stage and risk score remained significant risk factors. (D) A nomogram based on independent prognostic factors. (E) ROC curves for 1, 3, and 5 years. (F) DCA curves for 1, 3, and 5 years. (G) Calibration curve for evaluating the predictive performance of the nomogram.

Abbreviations: DCA: Decision curve analysis; ROC: Receiver operating characteristic.

Interestingly, only *ADH1B* was remarkably associated with resting memory CD4 T cells, monocytes, and resting mast cells (Figures 7D and A2). In summary, there were more types of immune cell infiltration in the low-risk group, and the increase of immune cell infiltration in tumor tissue was associated with longer patient survival. We also found that *ADH1B*, a metabolism-related gene, was significantly associated with various immune cells.

Subsequently, we discovered that the copy number on chromosomes 1, 5, 7, 8, 11, 12, 13, and 17 significantly increased, while the copy number on chromosomes 9 and 15 was remarkably decreased in high-risk groups. In the low-risk group, significant copy number amplification occurred on chromosomes 8, 9, and 12, while chromosome deletion occurred on chromosomes 1, 5, 9, and 15 (Figure 7E).

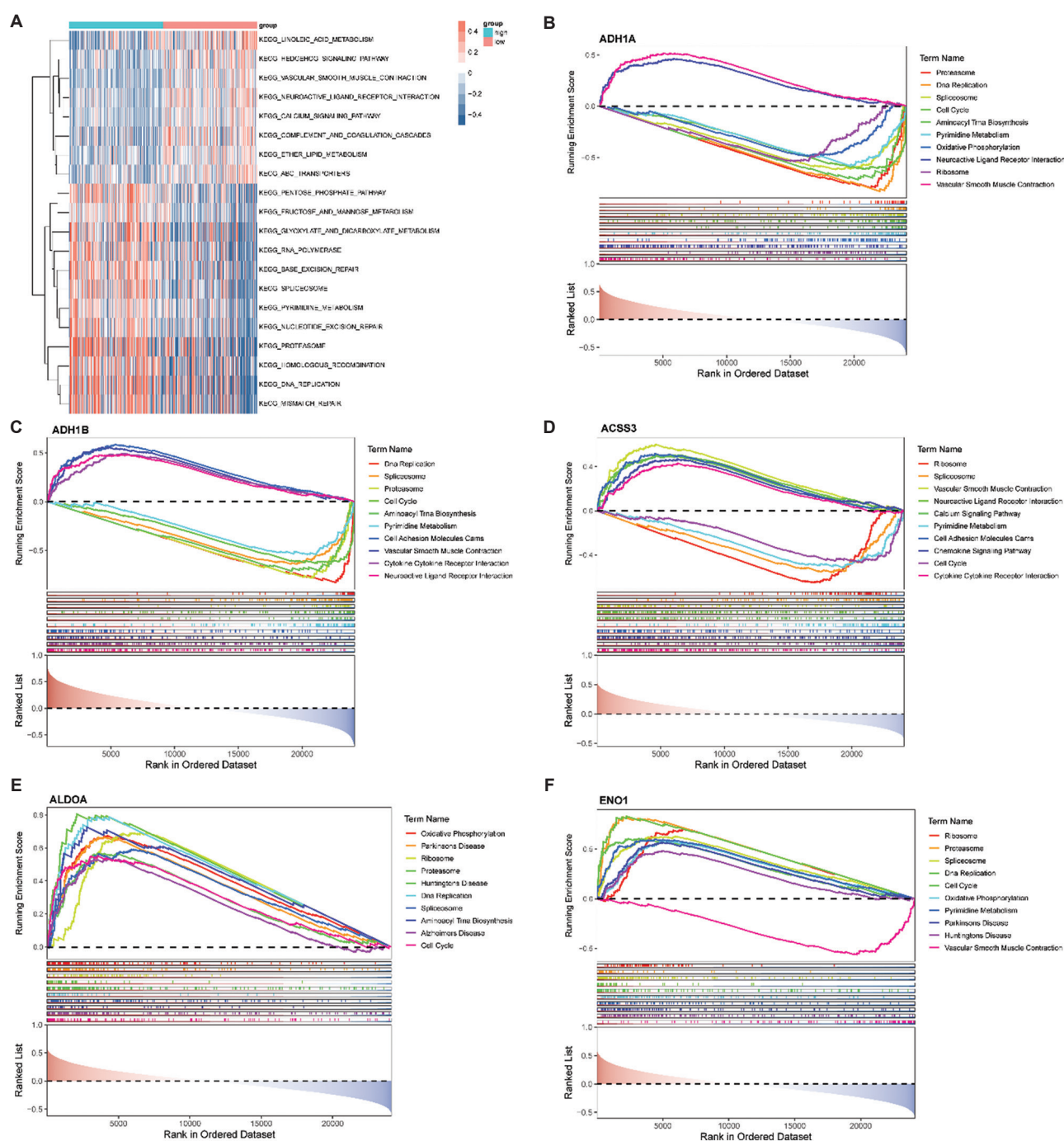


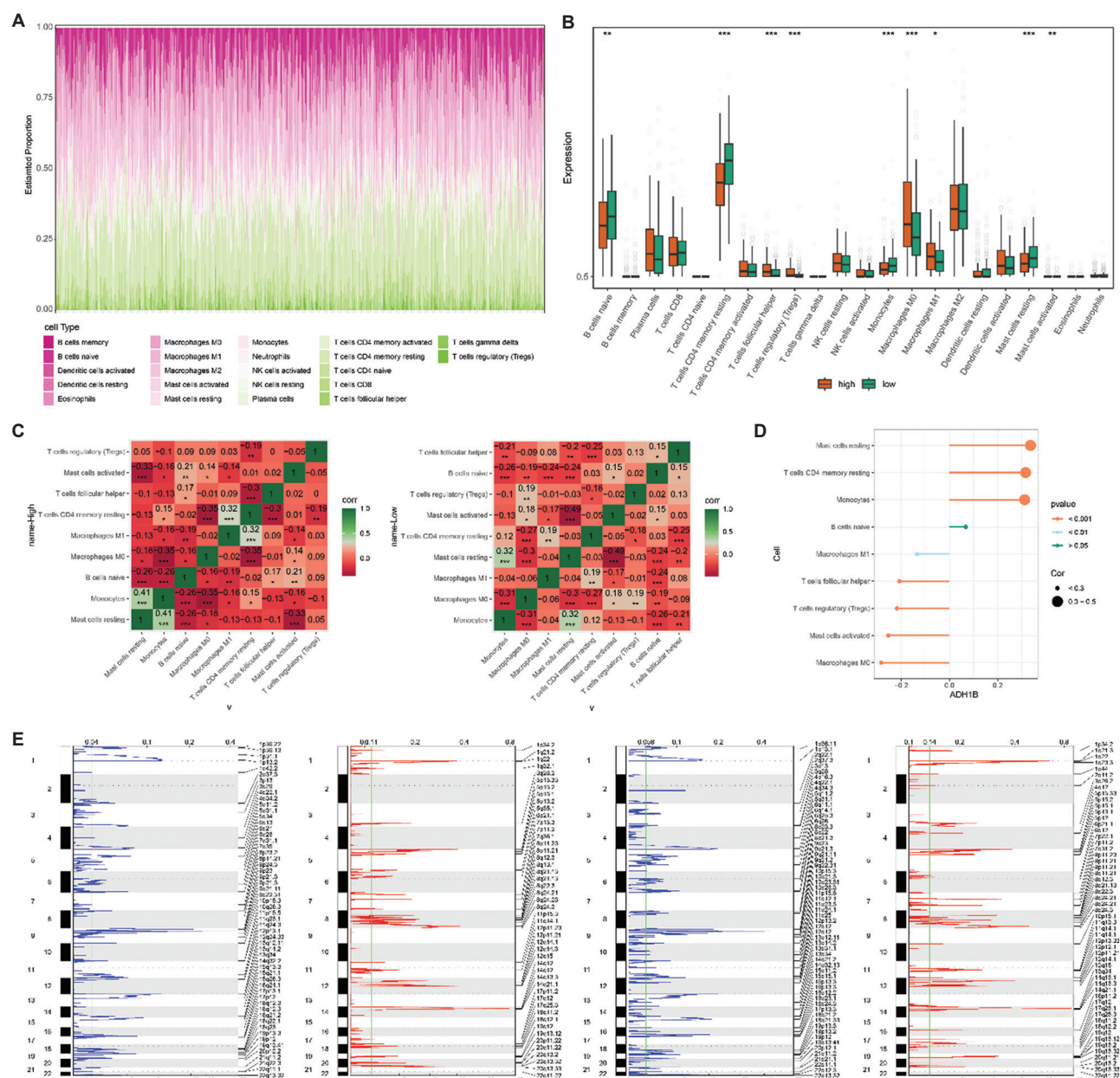
Figure 6. Functional enrichment of prognostic genes. (A) GSVA analyzes heat maps. Darker orange colors indicate higher positive correlation coefficients; darker blue colors indicate higher negative correlation coefficients. Enrichment differences in the KEGG pathway concentration can be observed between samples of the high- and low-risk groups. (B-F) Plot of GSEA results for *ADH1A*, *ADH1B*, *ACSS3*, *ALDOA*, and *ENO1*.

Abbreviations: GSEA: Gene set enrichment analysis; GSVA: Gene set variation analysis; KEGG: Kyoto Encyclopedia of Genes and Genomes.

3.8. Analysis of the TFs-mRNA-miRNA network in LUAD

The 23 miRNAs, four prognostic genes, and nine TFs were applied to establish a regulatory network. The *ADH1A* gene was not included in the network because no corresponding

regulatory miRNA was predicted. Among them, *ADH1B* was associated with hsa-mir-335-5p and hsa-mir-381-3p; *ACSS3* was only associated with hsa-mir-222-3p; *ENO1* and *ALDOA* were associated with most miRNAs (hsa-mir-200b-5p, mir-16-5p, and hsa-mir-98-5p)



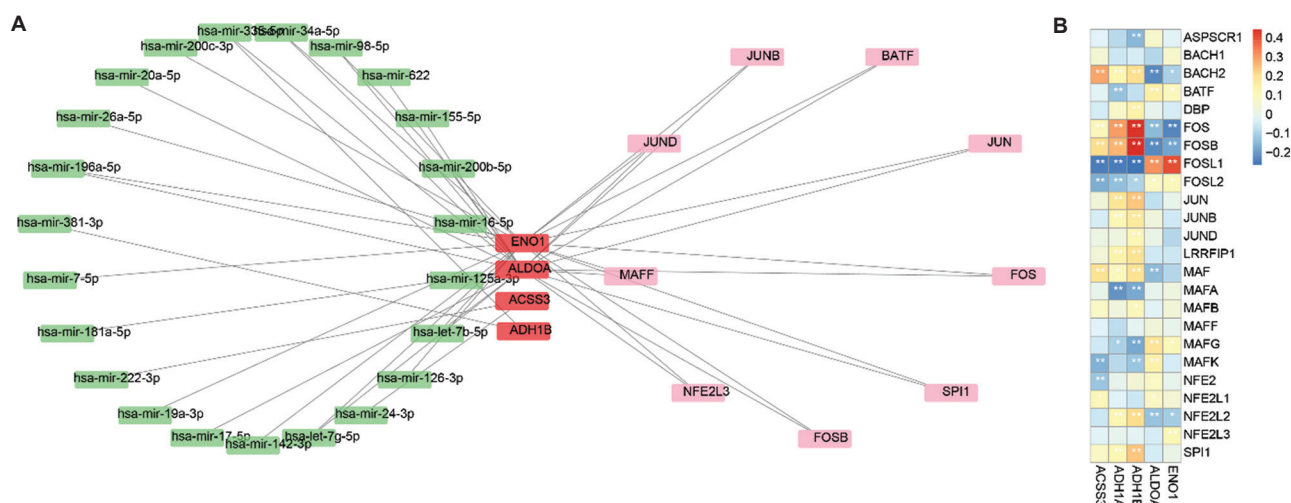


Figure 8. Analysis of the TF-mRNA-miRNA network in LUAD. (A) The TF-mRNA-miRNA regulatory network. Green represents miRNA, red represents prognostic genes, and pink represents TF. *ALDOA* and *ENO1* overlap with many miRNAs and TFs, suggesting that they may be the target genes of miRNAs or the regulatory binding genes of TFs. For example, mir-16-5p may regulate *ENO1* expression by binding to the mRNA of *ENO1*. Among them, *ADH1B* was only associated with hsa-mir-335-5p and hsa-mir-381-3p; *ACSS3* was only associated with hsa-mir-222-3p. (B) Heatmap for correlation analysis between prognostic genes and TF.

Abbreviations: LUAD: Lung adenocarcinoma; TF: Transcription factor.

the clinical tumor samples ($p < 0.05$), whereas *ALDOA* and *ENO1* exhibited markedly higher expression (Figure 9C). These results were consistent with the trends observed in the dataset.

4. Discussion

The emergence of transcriptomics has brought about a significant shift in the study of lung cancer mechanisms. This enables a better classification of tumor heterogeneity and provides patients with more accurate treatment options. Tumor cells change their metabolic pathways to meet the needs of rapid proliferation and survival. These metabolic changes not only support tumor growth but also affect the tumor microenvironment and therapeutic response. Exploring the key events in tumor metabolism is significant for understanding tumor mechanisms. In this work, we screened DEGs based on TCGA-LUAD, combined module genes obtained from WGCNA, and extracted carbohydrate and LRGs, consequently identifying 20 candidate genes. Subsequent enrichment analyses investigated their possible involvement in biological functions. Using PPI networks and machine learning, five prognostic genes (*ADH1A*, *ADH1B*, *ALDOA*, *ENO1*, and *ACSS3*) were filtered, and a relevant risk model was constructed to evaluate the overall survival (OS) of LUAD patients accurately. Furthermore, we conducted GSEA, GSEA, immune-infiltration analysis, and CNV analysis to explore the potential molecular mechanisms and prognostic value of LUAD.

The potential mechanism of these carbohydrate and LRGs is diverse. The alcohol dehydrogenase (ADH) type 1A gene (*ADH1A*) is a member of the ADH gene family. A previous study revealed that the genetic variation of *ADH5* may result in decreased expression of *ADH1A*, leading to impaired alcohol metabolism and an increased susceptibility to esophageal squamous cell carcinoma among individuals who consume alcohol.³⁰ In addition, *ADH1A* is closely related to tumor progression. In gastric cancer, *ADH1A* regulates the malignant characteristics and immune microenvironment of gastric cancer cells and promotes the transformation of macrophages to M1 phenotype.³¹ In breast cancer, *ADH1A* has become a potential prognostic marker by affecting cell migration, invasion, and changes in the tumor microenvironment.³² One study revealed that exosomal miR-2682-5p inhibited non-small cell lung cancer (NSCLC) cell viability and migration through the HDAC1/*ADH1A* axis,³³ and the upregulation of *ADH1A* inhibited cell proliferation and migration.

ADH1B is a member of the ADH family and exhibits high expression in the liver and adipose tissue. Studies have demonstrated that *ADH1B* plays an important role in the metabolism of pyruvate associated with breast cancer.³⁴ *TOP2A* and *ADH1B* can be used as diagnostic markers for LUAD and lung squamous cell carcinoma (LUSC), but only as independent prognostic factors for LUAD. In addition, both genes may be involved in lipid metabolism in LUAD patients.³⁵ The study also found that high expression

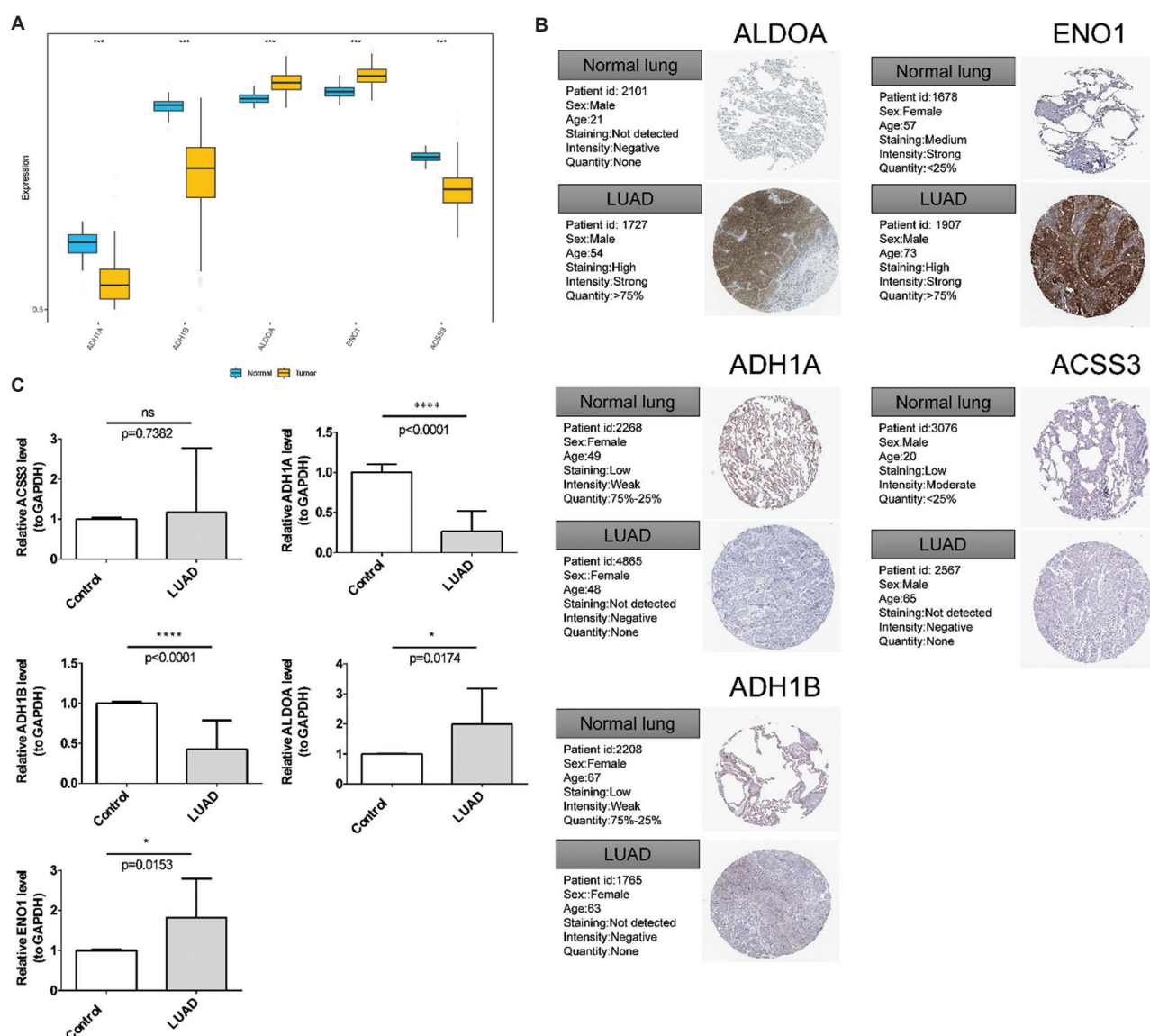


Figure 9. Expression validation of prognostic genes. (A) Expression of prognostic genes in the TCGA-LUAD dataset. (B) Pathologic images of prognostic genes. *ENO1* and *ALDOA* were highly expressed in tumor tissue and lowly expressed in normal lung tissue. *ADH1A*, *ADH1B*, and *ACSS3* were not detected in tumor tissue. (C) The qPCR validation of prognostic genes was performed in 10 pairs of LUAD patients with cancer and adjacent tissues; the results indicated that there were statistically significant differences in the expression of *ADH1A*, *ADH1B*, *ALDOA*, and *ENO1* in cancer and adjacent tissues, while there was no significant difference in the expression of *ACSS3*, which was likely due to the small sample size.

Abbreviations: LUAD: Lung adenocarcinoma; qPCR: Quantitative polymerase chain reaction.

of *ADH1B* may inhibit the malignant progression of pancreatic cancer by reducing cancer cell proliferation, thereby improving immune cell infiltration and reducing the mutation rate.³⁶ Single-cell RNA sequencing and histological assessment indicated that aggressive LUADs are characterized by a decreased number of *ADH1B*⁺ cancer-associated fibroblasts (CAFs) compared to indolent tumors. Survival analysis demonstrated that high expression of *ADH1B* is associated with better survival of LUAD patients.³⁷ The high expression of *ADH1B* is

associated with less aggressive features and a favorable prognosis.³⁶ Our data analysis suggests that both *ADH1A* and *ADH1B* are expressed at low levels in the high-risk group, and PCR confirmed that they are expressed at low levels in the tumor tissue, with statistically significant results, suggesting that they may be protective factors for LUAD.

Another protective factor identified in our study is acetyl-CoA synthetase short-chain family member 3 (*ACSS3*), which is expressed in the liver, kidney, lung,

and fat tissue, and participates in lipid and carbohydrate metabolism. Increased expression of *ACSS3* resulted in the accumulation of lipid droplets, while enhanced glycolysis led to an increase in extracellular lactic acid levels in A549 cell.³⁸ It has been reported that *ACSS3* significantly impacts the progression of gastric cancer (GC) and can enhance the 5-year OS rate in GC patients.³⁹ Proteomic analysis identified that *ACSS3* expression was decreased in IPF patients.³⁸ In prostate cancer, the downregulation of *ACSS3* expression leads to lipid droplet accumulation and increased *de novo* androgen synthesis within the tumor and is strongly associated with unfavorable prognosis.⁴⁰ By studying the promoter of the *ACSS3* gene, a study has identified multiple sites where TFs (especially *C/EBPα*) bind to factors associated with the initiation of starvation-related signaling. This suggests that the *C/EBPα*-*ACSS3* interaction may be critical for the regulation of cancer cells under energy-deprived stress conditions.³⁹ This study, based on the TCGA-LUAD dataset, found that *ACSS3* expression was downregulated in tumor samples, but qRT-PCR demonstrated no significant difference, which may be due to sample variability, experimental error, etc. Therefore, future studies should further consider the representativeness of the samples while exploring the regulatory mechanisms of *ACSS3* expression to better understand its role in the development of LUAD.

Alpha-enolase (*ENO1*), also known as 2-phosphate D-glycerol hydrolase, is a tumor protein located on the cell surface and in the cytoplasm,^{41,42} and it is a crucial enzyme in glycolysis. The long non-coding RNA (lncRNA) *NMRAL2P* inhibits the degradation of *ENO1* and may help cancer cells survive oxidative stress.⁴³ In line with our investigation, *ENO1* is overexpressed in 70% of cancers globally, thereby establishing the diagnostic and prognostic significance of *ENO1* overexpression across diverse tumor types.^{41,44-48} *ENO1* plays a key role in the malignant progression of bladder cancer and is closely related to the immune microenvironment of the tumor.⁴⁹ Other studies have found that *ENO1* expression affects the metabolism, proliferation, and migration of LUAD tumor cells through the regulation of circ-*ENO1*.⁵⁰ In cancer cells, *ENO1* is a critical player in the glycolytic pathway, primarily due to its function in transforming 2-phosphoglycerate into phosphoenolpyruvate, which is essential for the manifestation of the Warburg effect.^{50,51} The monoclonal antibody 12C7 demonstrates anti-tumor activity, with research confirming its target antigen as *ENO1*. Upregulation of *ENO1* expression has been reported to enhance the self-renewal, growth, and invasive capabilities of lung cancer stem cells through the AMPK/mTOR pathway.⁵² In our study, we found that *ENO1* was negatively correlated with *FOS*, and it was

significantly enriched in the ribosome, proteasome, and spliceosome in GSEA. Meanwhile, *ENO1* and *ALDOA* were associated with most miRNAs and TFs, suggesting that they play an important role in the post-transcriptional regulation mechanism of the tumor.

Aldolase A (*ALDOA*) is an aldolase isoenzyme encoded by three distinct genes.⁵³ It was found that *ALDOA* is an important target of lactylation, and lactation modification significantly affects its enzyme activity, which may play an important role in cell metabolism by regulating the glycolysis pathway.⁵⁴ The *ALDOA* axis promotes the progression of colon cancer by regulating cancer cell metabolism.⁵⁵ Kaplan–Meier analysis revealed that elevated *ALDOA* levels correlated with a poor prognosis in colorectal cancer patients.⁵⁶ Results from seahorse extracellular flux analysis indicated that *ALDOA* depletion significantly inhibited basic glycolytic capacity. The mRNA and protein expression of *ALDOA* were higher in LUAD than in normal tissues. The overexpression of *ALDOA* was significantly correlated with the high TNM stage. In addition, the copy number alterations of *ALDOA* were correlated with three immune cell infiltration levels.⁵⁷

Recent studies have revealed that *ALDOA* acts as an oncogene, promoting the glycolysis of cancer cells. Its upregulation is closely associated with the initiation, progression, metastatic potential, and unfavorable prognosis of diverse tumors.⁵⁸ Similarly, Chen *et al.*⁵⁹ also discovered that *ALDOA* can suppress DNA repair in pancreatic cancer, reversing DNA damage-induced cell cycle arrest and promoting the initiation and progression of cancer. *ALDOA* has been validated as a candidate oncogenic protein in a variety of cancers. Furthermore, Lu *et al.*,⁵⁷ through a sequence of survival prognosis assessments, determined that *ALDOA* acts as a promising prognostic biomarker and treatment target in LUAD. Besides that, *ALDOA* is a key enzyme involved in lung cancer metabolic reprogramming and metastasis, and it can be used as an effective therapeutic target for lung cancer.⁶⁰

The prognostic model for LUAD, constructed based on five core biomarkers (*ALDOA*, *ENO1*, *ACSS3*, *ADH1A*, and *ADH1B*), has demonstrated consistent and excellent performance in both the training and validation sets. Kaplan–Meier analysis confirmed a significant survival difference between the high- and low-risk groups ($p < 0.05$), with the high-risk group exhibiting a lower survival rate. The heatmap indicates that *ALDOA* and *ENO1* are highly expressed in the high-risk group, while *ACSS3*, *ADH1A*, and *ADH1B* are highly expressed in the low-risk group. The AUC values of the nomogram for survival prediction at 1, 3, and 5 years all exceed 0.6, indicating that our

model can effectively predict the survival status of LUAD patients. Further analysis revealed that risk scores and cancer staging are independent prognostic factors and high predictive accuracy and clinical applicability are demonstrated through constructed calibration plots, ROC curves, and DCA curves. This provides strong support for the early identification of high-risk LUAD patients and personalized treatment strategies. The high- and low-risk groups distinguished by our prediction model displayed significant differences in terms of immune cell infiltration, suggesting that different metabolic genes affect immune cell infiltration. In the high- and low-risk groups, there were also significant differences in CNV, suggesting that the genes we screened were involved in immune cell infiltration and the regulation of CNV.

The GSEA results demonstrated significant enrichment of these five biomarkers in pathways that are intricately linked to tumor initiation and progression. Notable pathways include DNA replication, spliceosome, oxidative phosphorylation, and ribosome, among others. Emerging mechanistic insights indicate that the disruption of ribosome biogenesis is involved in a broader spectrum of processes, contributing significantly to the onset and advancement of most spontaneously occurring cancers.⁶¹ Within cancer cells, there exists a unique type of ribosome, known as the cancer ribosome, which can enhance oncogenic translation programs to promote metabolic reprogramming and regulate cellular functions.⁶² In 2022, a comprehensive genome-wide CRISPR/Cas9 knockout screen was carried out to improve understanding of how ribosomal proteins and factors involved in ribosome biogenesis are transcriptionally regulated in mammals.⁶³ Genomic instability is a hallmark of cancer, and precise DNA replication is fundamental for the accurate copying and transmission of genetic information. DNA damage and replication defects can occur under constant pressure from endogenous and exogenous factors.⁶⁴

High levels of ENO1 are closely linked to DNA replication and the cell cycle. In contrast, low levels of ENO1 can disrupt the energy supply and metabolic balance of tumor cells, inhibit DNA replication, and prevent normal tumor cell growth and division.^{65,66} Meanwhile, mutations in core components of the spliceosome are frequently associated with cell- or tissue-specific manifestations of various diseases. Aberrant splicing is closely linked to the development of cancer, and spliceosome-targeted therapies have emerged as an effective anti-cancer strategy for patients with splicing defects.⁶⁷⁻⁶⁹ *KCNQ1OT1* acts as a competitive endogenous RNA to target the 3'UTR of *ALDOA* during the metabolic switch from oxidative phosphorylation to aerobic glycolysis, thereby stimulating

the expression of *ALDOA* in the Warburg effect by adsorbing miR-34c-5p.⁷⁰ We also used multiple online software to predict the miRNA correlation of these five genes, suggesting that several miRNAs have binding sites with ENO1 and ALDOA. These predictions can be further validated through *in vitro* experiments to explore the post-transcriptional regulatory mechanisms of these genes. The high- and low-risk groups predicted by these five genes exhibit distinct biological features in GSEA, CNV, and immune-infiltration analyses, indicating that the prognostic model composed of key genes related to lactate and carbohydrate metabolism is valuable for predicting the prognosis of LUAD.

In summary, this study identified and validated five reliable prognostic genes for LUAD and that ENO1 and ALDOA are the core enzymes of glycolysis. The high expression of ENO1 and ALDOA in tumor tissues may play a role in promoting the production of lactic acid, maintaining the local hypoxia of the tumor, and affecting the infiltration of immune cells in the tumor. We intend to explore new ideas in the metabolism of tumor nutrient supply. These results provided a valuable theoretical basis for diagnosing and prognosticating LUAD. However, it should be noted that this work has some limitations. The specific mechanisms by which *ADH1A*, *ADH1B*, *ALDOA*, *ENO1*, and *ACSS3* impact the progression of LUAD are still not fully understood. Although we have preliminarily confirmed the expression levels of these genes through qPCR and explored the post-transcriptional regulatory mechanisms, further investigations are warranted to systematically explore their regulatory mechanisms both *in vivo* and *in vitro*. In addition, the uneven sample size is also a challenge. In unbalanced data, models may tend to predict dominant categories, resulting in weaker predictive power for a few categories, thereby creating the risk of underfitting or overfitting. To address the bias caused by sample imbalance, we plan to use a resampling technique or weighted loss function to balance the categories in the future to ensure the reliability of the results.

5. Conclusion

Our study identified five key prognostic genes (*ADH1A*, *ADH1B*, *ALDOA*, *ENO1*, and *ACSS3*) linked to carbohydrate and lactic acid metabolism in LUAD, providing a theoretical basis for exploring novel therapeutic targets and improving clinical outcomes for LUAD patients.

Acknowledgments

We would like to extend our thanks to all colleagues who have provided assistance and support throughout the

research process. Their collaboration and encouragement have been invaluable to our work. We also thank Professor Xiansheng Liu, Min Xie, and Shuang Wei (Tongji Hospital, Wuhan) for their technical advice.

Funding

None.

Conflict of interest

The authors declare that they do not have competing interests.

Author contributions

Conceptualization: Zhiping Zhao

Formal analysis: Jiande Cheng

Investigation: Yanyan Hao

Methodology: Jiande Cheng

Writing – original draft: Zhiping Zhao

Writing – review & editing: Jiande Cheng, Yanyan Hao

Ethics approval and consent to participate

This study was performed in accordance with the principles of the Declaration of Helsinki and approved by the Shanxi Bethune Hospital Medical Ethics Committee (2024/4/10/YXLL-2024 – 082). Informed consent was obtained from all participants.

Consent for publication

The tissue specimens were sourced from the archived specimens of the department. The cases were selected from those who had signed the informed consent form upon admission.

Availability of data

Data analyzed in this study have been deposited in the TCGA (<https://www.cancer.gov/ccg/research/genome-sequencing/tcga>), MSigDB (<https://www.gsea-msigdb.org/gsea/msigdb/index.jsp>), and GEO (<https://www.ncbi.nlm.nih.gov/gds>) with the login number GSE31210.

References

- Chen Y, Tang L, Huang W, Zhang Y, Abisola FH, Li L. Identification and validation of a novel cuproptosis-related signature as a prognostic model for lung adenocarcinoma. *Front Endocrinol (Lausanne)*. 2022;13:963220. doi: 10.3389/fendo.2022.963220
- Travis WD, Brambilla E, Noguchi M, *et al.* International association for the study of lung cancer/american thoracic society/european respiratory society international multidisciplinary classification of lung adenocarcinoma. *J Thorac Oncol*. 2011;6(2):244-285. doi: 10.1097/JTO.0b013e318206a221
- Nguyen TT, Lee HS, Burt BM, *et al.* A lepidic gene signature predicts patient prognosis and sensitivity to immunotherapy in lung adenocarcinoma. *Genome Med*. 2022;14(1):5. doi: 10.1186/s13073-021-01010-w
- Zhang L, Zhang Z, Yu Z. Identification of a novel glycolysis-related gene signature for predicting metastasis and survival in patients with lung adenocarcinoma. *J Transl Med*. 2019;17(1):423. doi: 10.1186/s12967-019-02173-2
- Seguin L, Durandy M, Feral CC. Lung adenocarcinoma tumor origin: A guide for personalized medicine. *Cancers*. 2022;14(7):1759. doi: 10.3390/cancers14071759
- Alizadeh J, Kavosi M, Singh N, *et al.* Regulation of autophagy via carbohydrate and lipid metabolism in cancer. *Cancers*. 2023;15(8):2195. doi: 10.3390/cancers15082195
- Cui X, Zhao J, Li G, *et al.* Blockage of EGFR/AKT and mevalonate pathways synergize the antitumor effect of temozolomide by reprogramming energy metabolism in glioblastoma. *Cancer Commun (Lond)*. 2023;43(12):1326-1353. doi: 10.1002/cac2.12502
- Chandel NS. Carbohydrate metabolism. *Cold Spring Harbor Perspect Biol*. 2021;13(1):a040568. doi: 10.1101/cshperspect.a040568
- Chang X, Liu X, Wang H, Yang X, Gu Y. Glycolysis in the progression of pancreatic cancer. *Am J Cancer Res*. 2022;12(2):861-872.
- Bannasch P. Modulation of carbohydrate metabolism during carcinogenesis. *Cancer Detect Prev*. 1986;9(3-4):243-249.
- Vaupel P, Schmidberger H, Mayer A. The Warburg effect: Essential part of metabolic reprogramming and central contributor to cancer progression. *Int J Radiat Biol*. 2019;95(7):912-919. doi: 10.1080/09553002.2019.1589653
- San-Millan I, Brooks GA. Reexamining cancer metabolism: Lactate production for carcinogenesis could be the purpose and explanation of the Warburg effect. *Carcinogenesis*. 2017;38(2):119-133. doi: 10.1093/carcin/bgw127
- Huang R, Zong X. Aberrant cancer metabolism in epithelial-mesenchymal transition and cancer metastasis: Mechanisms in cancer progression. *Crit Rev Oncol Hematol*. 2017;115:13-22. doi: 10.1016/j.critrevonc.2017.04.005
- Certo M, Tsai CH, Pucino V, Ho PC, Mauro C. Lactate

- modulation of immune responses in inflammatory versus tumour microenvironments. *Nat Rev Immunol*. 2021;21(3):151-161.
doi: 10.1038/s41577-020-0406-2
15. Gu J, Zhou J, Chen Q, *et al*. Tumor metabolite lactate promotes tumorigenesis by modulating MOESIN lactylation and enhancing TGF- β signaling in regulatory T cells. *Cell Rep*. 2022;39(12):110986.
doi: 10.1016/j.celrep.2022.110986
 16. Ye L, Jiang Y, Zhang M. Crosstalk between glucose metabolism, lactate production and immune response modulation. *Cytokine Growth Factor Rev*. 2022;68:81-92.
doi: 10.1016/j.cytogfr.2022.11.001
 17. Chen XS, Li LY, Guan YD, Yang JM, Cheng Y. Anticancer strategies based on the metabolic profile of tumor cells: therapeutic targeting of the Warburg effect. *Acta Pharmacol Sin*. 2016;37(8):1013-1019.
doi: 10.1038/aps.2016.47
 18. Yang Y, Yang Y, Liu J, *et al*. Establishment and validation of a carbohydrate metabolism-related gene signature for prognostic model and immune response in acute myeloid leukemia. *Front Immunol*. 2022;13:1038570.
doi: 10.3389/fimmu.2022.1038570
 19. Langfelder P, Horvath S. WGCNA: An R package for weighted correlation network analysis. *BMC Bioinformatics*. 2008;9:559.
doi: 10.1186/1471-2105-9-559
 20. Love MI, Huber W, Anders S. Moderated estimation of fold change and dispersion for RNA-seq data with DESeq2. *Genome Biol*. 2014;15(12):550.
doi: 10.1186/s13059-014-0550-8
 21. Ma X, Zhang L, Huang D, *et al*. Quantitative radiomic biomarkers for discrimination between neuromyelitis optica spectrum disorder and multiple sclerosis. *J Magn Reson Imaging*. 2019;49(4):1113-1121.
doi: 10.1002/jmri.26287
 22. Yu G, Wang LG, Han Y, He QY. clusterProfiler: An R package for comparing biological themes among gene clusters. *OMICS*. 2012;16(5):284-287.
doi: 10.1089/omi.2011.0118
 23. Wang S, Su W, Zhong C, *et al*. An Eight-CircRNA assessment model for predicting biochemical recurrence in prostate cancer. *Front Cell Dev Biol*. 2020;8:599494.
doi: 10.3389/fcell.2020.599494
 24. Zhou RS, Zhang EX, Sun QF, *et al*. Integrated analysis of lncRNA-miRNA-mRNA ceRNA network in squamous cell carcinoma of tongue. *BMC Cancer*. 2019;19(1):779.
doi: 10.1186/s12885-019-5983-8
 25. Zheng Y, Wen Y, Cao H, *et al*. Global characterization of immune infiltration in clear cell renal cell carcinoma. *Oncotargets Ther*. 2021;14:2085-2100.
doi: 10.2147/OTT.S282763
 26. Hanzelmann S, Castelo R, Guinney J. GSEA: Gene set variation analysis for microarray and RNA-seq data. *BMC Bioinform*. 2013;14:7.
doi: 10.1186/1471-2105-14-7
 27. Ritchie ME, Phipson B, Wu D, *et al*. limma powers differential expression analyses for RNA-sequencing and microarray studies. *Nucleic Acids Res*. 2015;43(7):e47.
doi: 10.1093/nar/gkv007
 28. Subramanian A, Tamayo P, Mootha VK, *et al*. Gene set enrichment analysis: A knowledge-based approach for interpreting genome-wide expression profiles. *Proc Natl Acad Sci U S A*. 2005;102(43):15545-15550.
doi: 10.1073/pnas.0506580102
 29. Pilon-Thomas S, Kodumudi KN, El-Kenawi AE, *et al*. Neutralization of tumor acidity improves antitumor responses to immunotherapy. *Cancer Res*. 2016;76(6):1381-1390.
doi: 10.1158/0008-5472
 30. Cui Q, Peng L, Wei L, *et al*. Genetic variant repressing ADH1A expression confers susceptibility to esophageal squamous-cell carcinoma. *Cancer Lett*. 2018;421:43-50.
doi: 10.1016/j.canlet.2017.12.020
 31. Ma J, Shi Y, Lu Q, Huang D. Inflammation-related gene ADH1A regulates the polarization of macrophage M1 and influences the malignant progression of gastric cancer. *J Inflamm Res*. 2024;17:4647-4665.
doi: 10.2147/JIR.S452670
 32. Chen C, Guo S, Chai W, *et al*. A comprehensive genome-based analysis identifies the anti-cancerous role of the anoikis-related gene ADH1A in modulating the pathogenesis of breast cancer. *Mol Genet Genom MGG*. 2024;299(1):108.
doi: 10.1007/s00438-024-02200-y
 33. Mao G, Mu Z, Wu D. Exosome-derived miR-2682-5p suppresses cell viability and migration by HDAC1-silence-mediated upregulation of ADH1A in non-small cell lung cancer. *Hum Exp Toxicol*. 2021;40(12_suppl):S318-S330.
doi: 10.1177/09603271211041997
 34. Li YS, Jiang HC. Integrating molecular pathway with genome-wide association data for causality identification in breast cancer. *Disco Oncol*. 2024;15(1):254.
doi: 10.1007/s12672-024-01125-7
 35. Yin D, Zhang Y, Li H, Cheng L. Association of TOP2A and ADH1B with lipid levels and prognosis in patients with lung adenocarcinoma and squamous cell carcinoma. *Clin Respir J*. 2023;17(12):1301-1315.

- doi: 10.1111/crj.13717
36. Chida K, Oshi M, Roy AM, Sato T, Endo I, Takabe K. Pancreatic ductal adenocarcinoma with a high expression of alcohol dehydrogenase 1B is associated with less aggressive features and a favorable prognosis. *Am J Cancer Res*. 2023;13(8):3638-3649.
 37. Vasiukov G, Zou Y, Senosain MF, *et al*. Cancer-associated fibroblasts in early-stage lung adenocarcinoma correlate with tumor aggressiveness. *Sci Rep*. 2023;13(1):17604.
doi: 10.1038/s41598-023-43296-3
 38. Wang L, Yuan H, Li W, *et al*. ACS3 regulates the metabolic homeostasis of epithelial cells and alleviates pulmonary fibrosis. *Biochim Biophys Acta Mol Basis Dis*. 2024;1870(2):166960.
doi: 10.1016/j.bbdis.2023.166960
 39. Chang WC, Cheng WC, Cheng BH, *et al*. Mitochondrial Acetyl-CoA synthetase 3 is biosignature of gastric cancer progression. *Cancer Med*. 2018;7(4):1240-1252.
doi: 10.1002/cam4.1295
 40. Zhou L, Song Z, Hu J, *et al*. ACS3 represses prostate cancer progression through downregulating lipid droplet-associated protein PLIN3. *Theranostics*. 2021;11(2):841-860.
doi: 10.7150/thno.49384
 41. Huang CK, Sun Y, Lv L, Ping Y. ENO1 and cancer. *Mol Ther Oncolytics*. 2022;24:288-298.
doi: 10.1016/j.omto.2021.12.026
 42. Zhang T, Sun L, Hao Y, *et al*. ENO1 suppresses cancer cell ferroptosis by degrading the mRNA of iron regulatory protein 1. *Nat Cancer*. 2022;3(1):75-89.
doi: 10.1038/s43018-021-00299-1
 43. Nie Q, Cao H, Yang J, Liu T, Wang B. Long non-coding RNA NMRAL2P promotes glycolysis and reduces ROS in head and neck tumors by interacting with the ENO1 protein and promoting GPX2 transcription. *PeerJ*. 2023;11:e16140.
doi: 10.7717/peerj.16140
 44. Altenberg B, Greulich KO. Genes of glycolysis are ubiquitously overexpressed in 24 cancer classes. *Genomics*. 2004;84(6):1014-1020.
doi: 10.1016/j.ygeno.2004.08.010
 45. Chang GC, Liu KJ, Hsieh CL, *et al*. Identification of alpha-enolase as an autoantigen in lung cancer: Its overexpression is associated with clinical outcomes. *Clin Cancer Res*. 2006;12(19):5746-5754.
doi: 10.1158/1078-0432.CCR-06-0324
 46. He P, Naka T, Serada S, *et al*. Proteomics-based identification of alpha-enolase as a tumor antigen in non-small lung cancer. *Cancer Sci*. 2007;98(8):1234-1240.
doi: 10.1111/j.1349-7006.2007.00509.x
 47. Fu QF, Liu Y, Fan Y, *et al*. Alpha-enolase promotes cell glycolysis, growth, migration, and invasion in non-small cell lung cancer through FAK-mediated PI3K/AKT pathway. *J Hematol Oncol*. 2015;8:22.
doi: 10.1186/s13045-015-0117-5
 48. Zhang L, Wang H, Dong X. Diagnostic value of wth, migration, and invasion in non-small cell lung cancer through FAK-mediati. *J Brasil Pneumol*. 2018;44(1):18-23.
 49. Zhao J, Huang S, Tan D, *et al*. PGM1 and ENO1 promote the malignant progression of bladder cancer via comprehensive analysis of the m6A signature and tumor immune infiltration. *J Oncol*. 2022;2022:8581805.
doi: 10.1155/2022/8581805
 50. Zhou J, Zhang S, Chen Z, He Z, Xu Y, Li Z. CircRNA-ENO1 promoted glycolysis and tumor progression in lung adenocarcinoma through upregulating its host gene ENO1. *Cell Death Dis*. 2019;10(12):885.
doi: 10.1038/s41419-019-2127-7
 51. Gao J, Zhao R, Xue Y, *et al*. Role of enolase-1 in response to hypoxia in breast cancer: exploring the mechanisms of action. *Oncol Rep*. 2013;29(4):1322-1332.
doi: 10.3892/or.2013.2269
 52. Shu X, Cao KY, Liu HQ, *et al*. Alpha-enolase (ENO1), identified as an antigen to monoclonal antibody 12C7, promotes the self-renewal and malignant phenotype of lung cancer stem cells by AMPK/mTOR pathway. *Stem cell Res Ther*. 2021;12(1):119.
doi: 10.1186/s13287-021-02160-9
 53. Kukita A, Yoshida MC, Fukushige S, *et al*. Molecular gene mapping of human aldolase A (ALDOA) gene to chromosome 16. *Human genetics*. 1987;76(1):20-26.
doi: 10.1007/BF00283044
 54. Wan N, Wang N, Yu S, *et al*. Cyclic immonium ion of lactyllysine reveals widespread lactylation in the human proteome. *Nature Methods*. 2022;19(7):854-864.
doi: 10.1038/s41592-022-01523-1
 55. Lin J, Xia L, Oyang L, *et al*. The POU2F1-ALDOA axis promotes the proliferation and chemoresistance of colon cancer cells by enhancing glycolysis and the pentose phosphate pathway activity. *Oncogene*. 2022;41(7):1024-1039.
doi: 10.1038/s41388-021-02148-y
 56. Sun L, Lu T, Jiang L, *et al*. ALDOA contributes to colorectal tumorigenesis and metastasis by targeting YAP. *Cell Death Discov*. 2025;10(1):489.
doi: 10.1038/s41420-024-02249-z
 57. Lu G, Shi W, Zhang Y. Prognostic implications and immune infiltration analysis of ALDOA in lung adenocarcinoma. *Front Genet*. 2021;12:721021.

- doi: 10.3389/fgene.2021.721021
58. Kuang Q, Liang Y, Zhuo Y, *et al.* The ALDOA metabolism pathway as a potential target for regulation of prostate cancer proliferation. *Onco Targets Ther.* 2021;14:3353-3366.
doi: 10.2147/OTT.S290284
 59. Chen H, Ye Z, Xu X, *et al.* ALDOA inhibits cell cycle arrest induced by DNA damage via the ATM-PLK1 pathway in pancreatic cancer cells. *Cancer Cell Int.* 2021;21(1):514.
doi: 10.1186/s12935-021-02210-5
 60. Chang YC, Chiou J, Yang YF, *et al.* Therapeutic targeting of aldolase A interactions inhibits lung cancer metastasis and prolongs survival. *Cancer Res.* 2019;79(18):4754-4766.
doi: 10.1158/0008-5472.CAN-18-4080
 61. Pelletier J, Thomas G, Volarević S. Ribosome biogenesis in cancer: New players and therapeutic avenues. *Nat Rev Cancer.* 2018;18(1):51-63.
doi: 10.1038/nrc.2017.104
 62. Elhamamsy AR, Metge BJ, Alsheikh HA, Shevde LA, Samant RS. Ribosome biogenesis: A Central player in cancer metastasis and therapeutic resistance. *Cancer Res.* 2022;82(13):2344-2353.
doi: 10.1158/0008-5472.CAN-21-4087
 63. Schwarz JD, Lukassen S, Bhandare P, *et al.* The glycolytic enzyme ALDOA and the exon junction complex protein RBM8A are regulators of ribosomal biogenesis. *Front Cell Dev Biol.* 2022;10:954358.
doi: 10.3389/fcell.2022.954358
 64. Zhu H, Swami U, Preet R, Zhang J. Harnessing DNA replication stress for novel cancer therapy. *Genes.* 2020;11(9):990.
doi: 10.3390/genes11090990
 65. Zhu W, Li H, Yu Y, *et al.* Enolase-1 serves as a biomarker of diagnosis and prognosis in hepatocellular carcinoma patients. *Cancer Manag Res.* 2018;10:5735-5745.
doi: 10.2147/CMAR.S182183
 66. Cancemi P, Buttacavoli M, Roz E, Feo S. Expression of alpha-enolase (ENO1), Myc promoter-binding protein-1 (MBP-1) and matrix metalloproteinases (MMP-2 and MMP-9) reflect the nature and aggressiveness of breast tumors. *Int J Mol Sci.* 2019;20(16):3952.
doi: 10.3390/ijms20163952
 67. Yang H, Beutler B, Zhang D. Emerging roles of spliceosome in cancer and immunity. *Protein Cell.* 2022;13(8):559-579.
doi: 10.1007/s13238-021-00856-5
 68. Bowling EA, Wang JH, Gong F, *et al.* Spliceosome-targeted therapies trigger an antiviral immune response in triple-negative breast cancer. *Cell.* 2021;184(2):384-403.e321.
doi: 10.1016/j.cell.2020.12.031
 69. Eymin B. Targeting the spliceosome machinery: A new therapeutic axis in cancer? *Biochem Pharmacol.* 2021;189:114039.
doi: 10.1016/j.bcp.2020.114039
 70. Shen Y, Xu J, Pan X, *et al.* LncRNA KCNQ1OT1 sponges miR-34c-5p to promote osteosarcoma growth via ALDOA enhanced aerobic glycolysis. *Cell Death Dis.* 2020;11(4):278.
doi: 10.1038/s41419-020-2485-1

Appendix

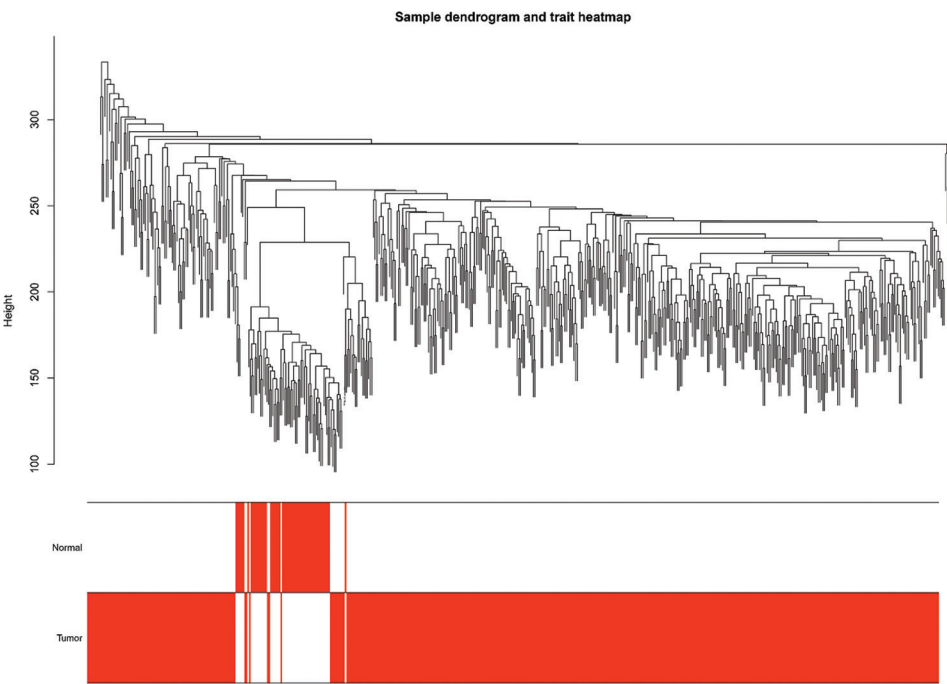


Figure A1. Sample clustering plot. Branches represent samples, and vertical coordinates represent the height of hierarchical clustering (top). The labels usually represent the samples (bottom).

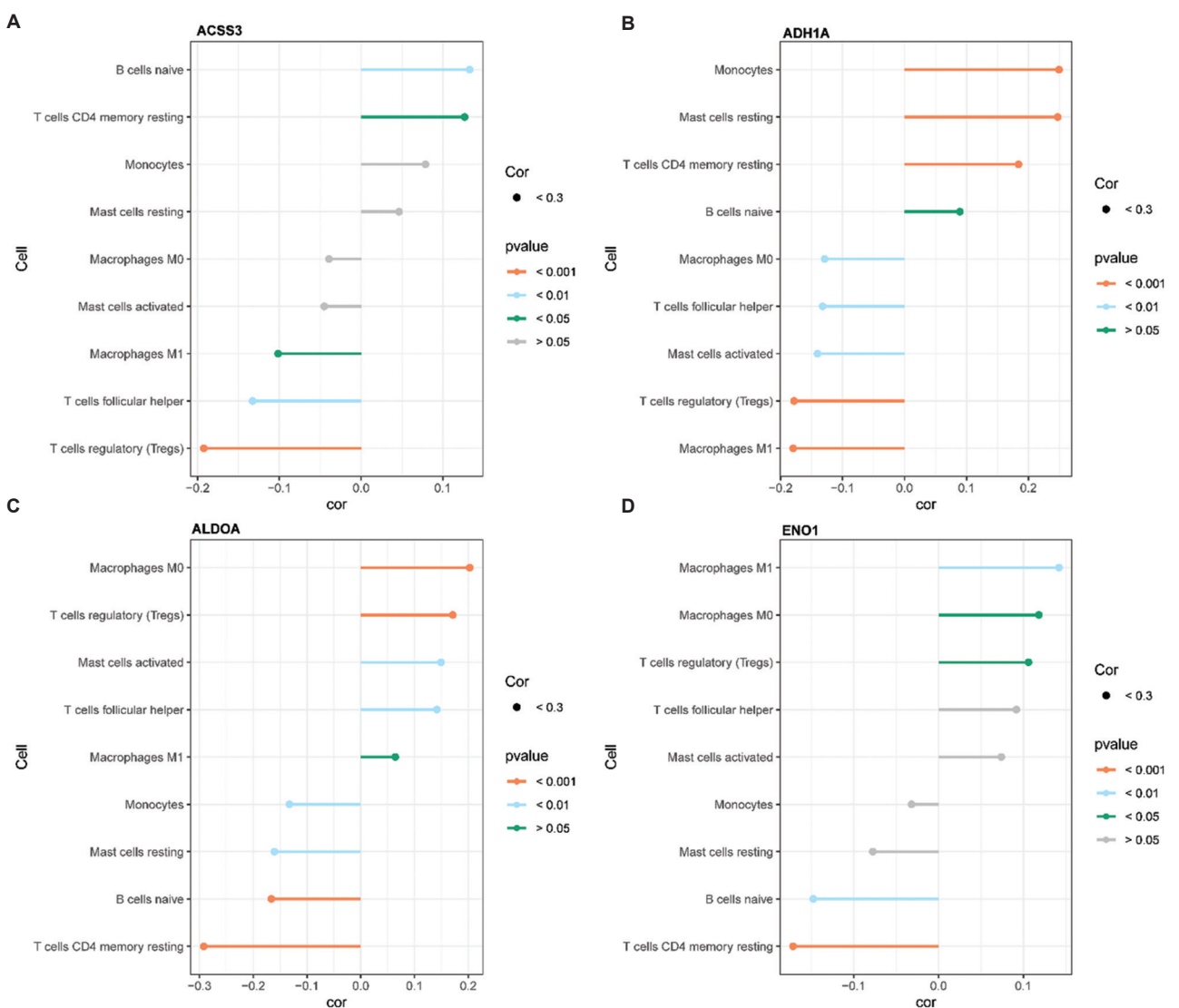


Figure A2. Lollipop plots for correlation analysis of key immune infiltrating cells with prognostic genes
Abbreviation: Cor: Correlation.